An Experimental and Modeling Investigation of Synthetic Jets in a Coflow Wake

by

Xi Xia and Kamran Mohseni

Reprinted from

International Journal of
Flow Control

Volume 3 · Number 1 · March 2011

Multi-Science Publishing
ISSN 1756-8250

An Experimental and Modeling Investigation of Synthetic Jets in a Coflow Wake

Xi Xia[1]* and Kamran Mohseni[1,2]†
[1] Department of Mechanical and Aerospace Engineering,
[2] Department of Electrical and Computer Engineering,
University of Florida, Gainesville, FL 32611

Abstract

A round synthetic jet injected in a coflow wake is investigated experimentally in order to estimate the spreading and decaying rates of the jet while compensating for the actuator wake. The flow field of the jet and wake is measured using hot-wire anemometry. The spatial evolution of the synthetic jet is modeled similarly to a continuous turbulent jet in a coflow with some modifications for the pulsatile nature of the synthetic jet and the wake behind the flow actuator. The model employs an integral formulation that conserves the excess momentum flux in the jet along with a hypothesis which asserts that the rate of growth of the shear layer is proportional to the velocity of the dominant eddies in the jet relative to the surroundings. The characteristic velocity and length scales are derived from a corresponding top hat velocity profile. The jet in the far field is observed to exhibit self-similar behavior, as distinguished by the overlapping of the excess mean velocity profiles if scaled by the self-similar variables. The streamwise variation of the centerline velocity shows good agreement with the proposed semi-empirical integral model. The verification of the theoretical model suggests that the decay of the non-dimensional relative velocity of the jet depends mostly on the spreading rate of the same synthetic jet in a quiescent environment. The spreading rate of the synthetic jet decreases as the coflow velocity increases. Finally, for a synthetic jet in a coflow wake, a larger actuator stroke ratio results in a faster velocity decay as well as an enhanced spreading rate.

Nomenclature

b_g	half width of jet for a Gaussian velocity profile
B	half width of jet for a top-hat velocity profile
d	diameter of orifice
f	frequency of oscillation
H	height of cavity
h	depth of orifice
K_e	excess kinematic momentum flux
β_g	jet spreading rate for gaussion profile
β	jet spreading rate for top-hat profile
L	length of slug
L/d	stroke ratio
Re	reynolds number
r	radial coordinate
T	time period of oscillation
U_j	mean jet exit velocity
u	streamwise jet velocity
U_a	local effective coflow velocity (uniform coflow velocity)

*Graduate Student, Department of Mechanical and Aerospace Engineering.
†W. P. Bushnell Endowed Professor, Department of Mechanical and Aerospace Engineering and Department of Electrical and Computer Engineering, Associate Fellow of the AIAA.

U_c	centerline jet velocity for a free synthetic jet
U_t	wind tunnel velocity
u_e	velocity in excess of the coflow velocity
ΔU_g	centerline excess velocity
ΔU	jet excess velocity for top-hat profile
V_d	driving voltage
x	axial coordinate
x_o	virtual origin
l^*	excess momentum length scale
U^*	scaled excess velocity for top-hat profile
B^*	scaled half width of jet for top-hat profile
x^*	scaled streamwise distance
ν	kinematic viscosity of fluid

A synthetic jet is a zero net mass flux (ZNMF) and fully pulsatile jet that results from the formation and interaction of vortex rings or pairs [1]. A common method of generating a synthetic jet is to apply a periodic pressure gradient across the orifice of a cavity. This affects the cyclic inception of a shear layer at the orifice edge, which in turn, rolls up into a vortex ring that travels downstream due to its induced velocity. Figure 1 shows a schematic of the suction and ejection strokes that constitute cycles in this synthesis. In this fashion, a train of vortex rings moves away from the orifice, whereupon they interact, and break down in a transition towards a turbulent jet directed downstream. This operational principle allows for a synthetic

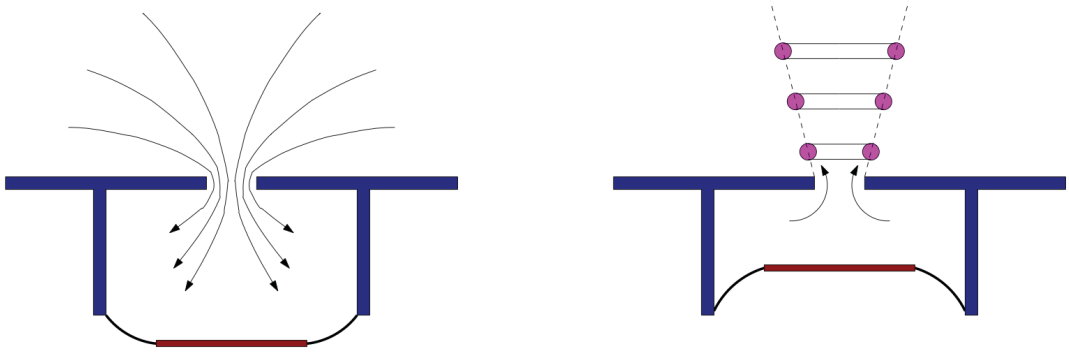

(a) Suction (b) Ejection

Figure 1: Schematic of synthetic jet operation displaying the suction and ejection strokes. (a) Suction; (b) Ejection.

jet to be synthesized entirely from the surrounding medium, while at the same time imparting a net momentum flux to the surrounding environment. In addition, the ability to influence the surrounding medium at a variety of scales has made synthetic jets attractive for a number of applications [2].

Flow control is the major area of application for synthetic jets; for example, some synthetic jet actuators have been designed to reduce drag by introducing disturbances into the boundary layer adjacent to a flow structure, thereby enhancing momentum transfer within the shear layer and forestalling separation [3, 4]. Similar concepts have been employed in underwater vehicle propulsion and low speed maneuvering [5, 6]. Micro synthetic jets have also been proposed for propulsion of tiny endoscopy capsules inside the human body [7, 8]. Finally, synthetic jets have been shown to modify the aerodynamic characteristics of airfoil surfaces [9, 10] and enhance aerodynamic lift of fixed wing micro air vehicles in wind tunnel tests [11].

Synthetic Jets in Coflow. In order to design synthetic jet actuators for these applications, a model of the evolution of the emerging jet is required. In practice, the surrounding medium is rarely stationary and may possess parallel, perpendicular or swirl velocity components. While most semi-empirical and numerical models of the mean velocity fields focus on jets injected into a quiescent environment [1, 12, 13, 14], less focus has been directed towards coflow or crossflow configurations [15, 16]. Considering that the characteristics of a jet changes if an external flow is present, this study is focused on extending a semi-empirical modeling technique for continuous jets to synthetic jets operating in a coflow

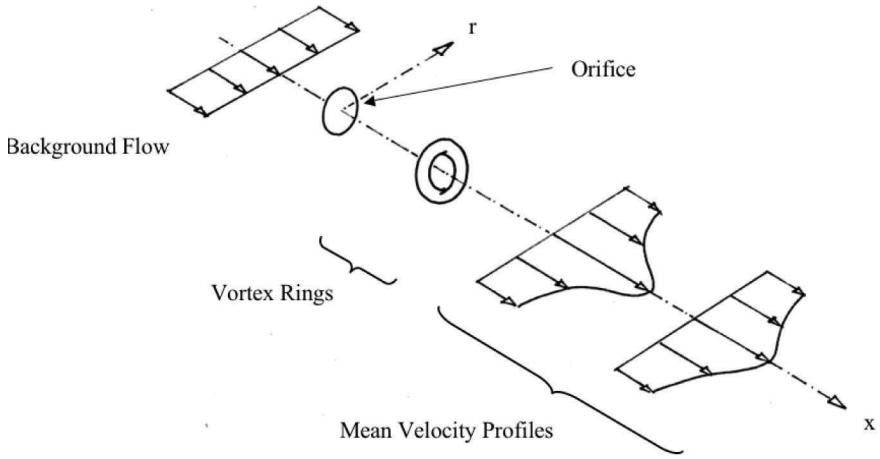

Figure 2: Schematic of the evolution of a round synthetic jet in a coflow, showing a vortex ring in the near field, and mean velocity profiles of the jet in the far field.

downstream of the actuator wake.

Figure 2 shows a schematic of a synthetic jet in an ideal coflow. The near field of the synthetic jet is typified by the presence of discrete coherent vortex rings and fully pulsatile flow. The effect of coflow on the formation of vortex rings, has been investigated and shown to reduce the strength of vorticity of the starting vortex rings and to delay the vortex pinch-off process [17]. Further downstream, the flow spreads further away from the orifice and breaks into a turbulent jet with many similarities to a turbulent continuous jet.

Synthetic jets in a quiescent environment share many features of their continuous jet counterparts. These include experimental self-similarity of the flow as inferred from the overlapping of the scaled mean and turbulent intensity profiles [1, 18]. In this investigation we will show that many of these similarities may be extended to the case of synthetic jets in coflow wakes. In the far field, the effect of the coflow on a continious turbulent jet is shown to enhance the advection of the jet, while reducing the jet spreading rate [19, 20, 21]. The counterpart of this region for a synthetic jet is the focus of this study.

The Proposed Modeling Technique. As synthetic jets exhibit several similarities to continuous jets [1, 2], here we develop a model for a synthetic jet in a coflow by modifying a similar model for continuous jets. Modeling a jet in a coflow involves predicting the velocity decay and spreading of the jet as it interacts with the background flow. Most models of continuous jets in a coflow assume that the flow is self-similar at some distance from the jet origin. This reduces the problem to one of solving for the streamwise variation of an appropriately chosen characteristic length and velocity scales in the jet. Two relevant equations are then required to determine these two unknowns. For the first equation, using an integral formulation, most models have assumed that the streamwise excess momentum flux is conserved, resulting in a relationship between the length and velocity scales. One additional equation is then required to determine the streamwise variation of the velocity and length scales. This is where several approaches have been proposed in the literature on continuous jets. One method employs a secondary momentum integral in conjunction with the Prandtl mixing length theory while assuming a constant eddy viscosity throughout the flow [22]. Despite the results being comparable to experimental data, the streamwise variation is not predicted correctly. This is attributed to the inaccurate of the constant eddy viscosity hypothesis. Another approach employs higher order moments of the momentum equation without using any phenomenological assumptions [23]. This model did not show good experimental agreement for weak jets or the far field of strong jets where the excess velocity was comparable to the coflow velocity. Another method applies a double integral method while employing a large eddy hypothesis, which essentially relates the Reynolds stresses to the shear strain rate through the length scales of the largest eddies in the shear flow [24]. Again, this model does not agree well with the experimental data. An alternative approach is to use an equation to relate the growth of the shear layer, and consequently the length scale, to the velocity scale in the flow based on the jet entrainment [25, 26]. It is found that this approach results in accurate predictions for weak jets only. In summary, these techniques for continuous jets all show poor performance at least in some flow regions and fail to offer a good agreement with experimental data over the entire range of the jet and coflow field

strengths. Recently, a model employing the conservation of excess momentum and an auxiliary equation for a spreading hypothesis has shown much better agreement with experimental data [21]. The key difference among these techniques lies in the selection of the characteristic length and velocity scales. The previous models derive the characteristic length and velocity scales directly from an assumed Gaussian-like mean velocity profile while an equivalent top hat velocity profile is defined and employed in [21]. Moreover, this new model agrees well with experimental data over a wide range of continuous jet strength. We will extend similar ideas to synthetic jets in a coflow wake here.

As mentioned previously, we have already developed a model for a synthetic jet in quiescent environment. Our model accounts for the enhanced spreading and decaying rates of a synthetic jet, caused by the pulsatile nature of the flow, through an enhanced eddy viscosity value[1]. This eddy viscosity is directly related to the momentum of the jet which is dictated by the actuator and its operating parameters. On the other hand, for modeling a synthetic jet in a background coflow, one requires to provide information about the coflow parameters as well. Furthermore, since actual synthetic jets have a finite dimension, a wake is expected downstream of the actuator. Information about the actuator wake is also expected to influence the result. Therefore, in this investigation, a model for synthetic jets in coflow, and more generally, in coflow wakes is proposed where the effect of the coflow on the jet is modeled while the impact of the actuator wake is properly addressed. This model was inspired by models of continuous jets in coflow which have been used to predict the mean behaviors of the jet and to identify the dominant parameters controlling the jet spreading and decay. These parameters are the coflow velocity and the jet momentum. Similar to extending the model of free continuous jets to synthetic jets, the validity of extending this model from continuous jets in a coflow to synthetic jets in a coflow requires the use of an enhanced eddy viscosity to account for the enhanced mixing and spreading rates of a synthetic jet. We also assume that the excess mean velocity profiles of a synthetic jet in coflow display self-similarity in the far field. This assumption is experimentally validated posteriori. After the model is established, experiments are conducted to study the jet flow field using a hot-wire anemometry. While a continuous coflow jet could be easily formed by placing the exit of a pipe connected to a pressurized fluid tank in a background flow, a synthetic jet is synthesized from the surrounding fluid itself. As a result, the entire jet actuator is required to be placed in the background flow. This introduces a new modeling challenge as the wake behind a synthetic jet actuator is significantly larger than a corresponding continuous jet setup, and therefore, additional compensations need to be made to resolve the coflow wakes instead of a uniform coflow.

This manuscript is organized as follows. Section 1 briefly outlines the self-similar model for a continuous jet in a coflow and addresses the changes that need to be made to account for using a synthetic jet in a coflow wake background. The experimental setup for the measurement of the velocity field is then described in Section 2. The results are presented and discussed in Section 3. Concluding remarks are summarized in Section 4.

1. THEORETICAL MODEL

In this section, we first review the theoretical framework for modeling a continuous jet in a uniform coflow [21]. We will then extend the model to the case of a synthetic jet in a coflow with significant actuator wake effects.

1.1. Continuous Jets in a Coflow

Figure 3 shows a schematic of the mean velocity profile in the far field of a turbulent jet formed from a round orifice of diameter d injected parallel to a free stream with a uniform velocity U_a. For modeling purposes, the far field of the jet in a coflow may be modeled as if it were generated by a continuous point source of momentum in a flow parallel to the jet. The velocity in excess of the coflow velocity at any position is then given by

$$u_e(x,r) = u(x,r) - U_a. \tag{1}$$

where x indicates the streamwise direction and r is the radial direction.

The excess velocity profile in the far field of a continuous turbulent jet is known to exhibit a self-

[1]This observation and the measurement and modeling of the enhanced eddy viscosity of a synthetic jet has been the focus of several publications from our group [13, 14, 27]

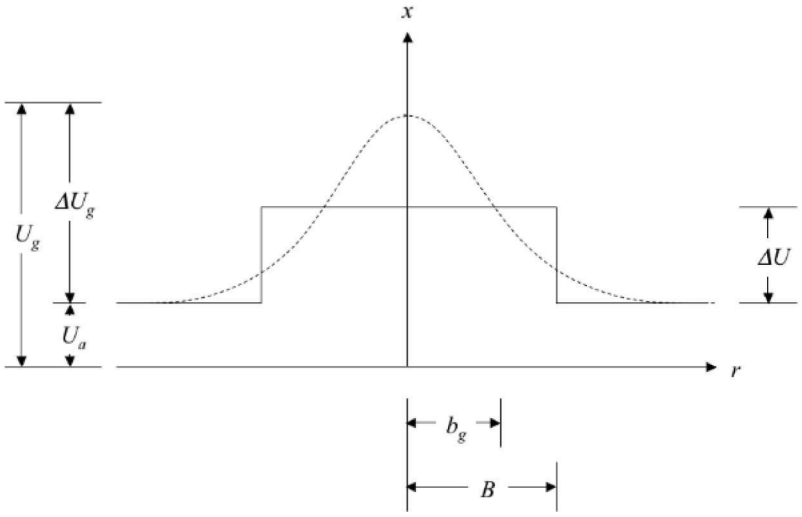

Figure 3: Schematic of the mean Gaussian and equivalent top-hat velocity profiles in a continuous jet in a uniform background flow.

similar behavior [19, 20] and to be well approximated by a Gaussian profile given by

$$\frac{u_e}{\Delta U_g} = e^{-\frac{r^2}{b_g^2}}. \tag{2}$$

where ΔU_g is the centerline excess velocity and b_g is the characteristic width of the jet, defined as the radial distance where $u_e = \frac{1}{e}\Delta Ug$. Using boundary layer approximations, it can be shown that the excess kinematic momentum flux, K_e, defined as

$$K_e = 2\pi\int_0^\infty uu_e r dr, \tag{3}$$

is conserved in the streamwise direction for a continuous jet in a coflow [28]. As the behavior of the jet is dependent primarily on K_e and U_a, an excess momentum length scale may be defined by

$$l^* = \frac{\sqrt{K_e}}{U_a}. \tag{4}$$

In this study, we make the assumption that the width and the mean strength of the excess velocity profile are the most relevant parameters for modeling a jet in a coflow. While a Gaussian velocity profile approximates well the real excess velocity distribution in the far field of a continuous jet, it carries more information than needed for our modeling purposes. To avoid unnecessary complications, in this study we limit ourselves to a top-hat excess velocity profile with only two main characteristic scales; namely, the width B and the amplitude ΔU. As seen shortly, this implies that the changes in the velocity profile may be rather simply characterized by two parameters of an equivalent top hat velocity profile (shown in Figure 3) that can be described as:

$$u_e = \begin{cases} \Delta U & r < B \\ 0 & r > B \end{cases}$$

The use of this top hat profile can be motivated by the need to identify proper velocity and width scales for the jet so that the spreading and decaying behaviors are modeled straightforwardly. Therefore, these characteristic scales are determined from a conservation prospective of the excess mass flux and excess momentum flux so that the large scale eddies with a length scale on the order of B are responsible for

jet spreading and they are advected with respect to the ambient coflow at a velocity of ΔU. The relationship between the top-hat and Gaussian profiles could be derived by equating their excess mass and excess momentum fluxes. These conditions are given by:

$$\pi B^2 \Delta U = 2\pi \int_0^\infty u_e r dr, \tag{5}$$

and

$$\pi B^2 \left(\Delta U + U_a\right) \Delta U = 2\pi \int_0^\infty u u_e r dr, \tag{6}$$

Solving the above equations for the velocity profile given in Eq. 2, yields

$$\Delta U = \frac{\Delta U_g}{2}, \tag{7}$$

and

$$B = \sqrt{2} b_g. \tag{8}$$

To relate the jet width to the jet velocity, it is assumed that the change in the width of the shear layer moving with the eddies is proportional to the relative velocity between the jet and the surroundings. That is

$$\frac{dB}{dt} = \left|U_a + \Delta U\right| \frac{dB}{dx} = \beta |\Delta U|, \tag{9}$$

where β is the proportionality factor and the characteristic velocity and length scales are obtained from the top hat velocity profile. Assuming that β remains constant for a given jet, the above relation should hold for a continuous jet in a quiescent environment in which case $U_a = 0$. Here, the spreading rate for this free continuous jet is designated as β_g, which is calculated from the characteristic jet width b_g. Therefore

$$\beta = \sqrt{2} \beta_g. \tag{10}$$

The conservation of excess momentum flux defined in Eq. 3 for the top hat velocity profile yields

$$K_e = \pi B^2 U \Delta U = \pi B^2 \left(\Delta U + U_a\right) \Delta U, \tag{11}$$

which, using Eq. 4, can be rearranged to

$$\left(\frac{\Delta U}{U_a}\right)^2 + \left(\frac{\Delta U}{U_a}\right) - \left(\frac{l^{*2}}{\pi B^2}\right) = 0. \tag{12}$$

The excess momentum Eq. 12 and the spreading hypothesis in Eq. 9 can be nondimensionalized to

$$U^{*2} + U^* - \frac{1}{\pi B^{*2}} = 0, \tag{13}$$

and

$$\frac{dB^*}{dx^*} = \sqrt{2} \beta_g \frac{U^*}{1 + U^*}, \tag{14}$$

where $U^* = \Delta U/U_a$, $B^* = B/l^*$, and $x^* = x/l^*$. The initial conditions for this set of equations can be written as $U_o^* = \Delta U_o/U_a$ and $B_o^* = B_o/l^*$ where U_o and B_o are the measured values at some convenient point in the turbulent far field region. Equations 13 and 14 are coupled differential equations which predict the streamwise evolution of the velocity magnitude and its spreading. This approach has been successfully employed in modeling continuous jets in a coflow [21].

1.2. Extending Continuous Jet Model to Synthetic Jets in a Quiescent Environment

The previous discussion demonstrates the need for a model that extends the continuous jet theory to synthetic jets. Actually, as will be discussed in the following section, there is a far field region for a synthetic jet that displays the same self-similarity that is seen in turbulent continuous jets. This provides the basis for the possibility of finding a self-similar solution for a synthetic jet in a similar approach as that for a continuous jet.

One classic self-similar solution for free continuous jets is the Schlichting [29] solution. The far field of a continuous jet may be thought of as being generated by a continuous point source of momentum in an infinite incompressible fluid. It is admissible to describe the mean velocities in the continuous jet by boundary layer equations. For a self-similar solution to the boundary layer equations to exist, the streamwise pressure gradient must be zero, whereupon a closed form solution for a laminar jet may be found [29]. It was later seen [30] that the turbulent jet could be modeled using the same differential equations that described the laminar jet, but with the laminar viscosity coefficient replaced by an effective eddy viscosity coefficient associated with the turbulent jet. Following along these lines it is hypothesized here that the mean velocity field of a synthetic jet may be modeled as a laminar free jet, so long as one uses an effective viscosity coefficient obtained empirically instead of the usual viscosity. Next, a round continuous jet model will be introduced and then the compatibility with a synthetic jet will be discussed.

In cylindrical coordinates the boundary layer equations with no pressure gradient are written as

$$\frac{\partial u}{\partial x} + \frac{\partial \upsilon}{\partial r} + \frac{\upsilon}{r} = 0, \text{ and } u\frac{\partial u}{\partial x} + \upsilon\frac{\partial u}{\partial r} = \frac{1}{\rho r}\frac{\partial (r\tau)}{\partial r}, \tag{15}$$

where u and υ are the streamwise and radial velocity components respectively, τ is the total shear stress, and ρ is the fluid density. The total shear stress may be related to the mean velocity using an eddy viscosity approximation

$$\tau = \rho(\nu + \varepsilon_\tau)\frac{\partial u}{\partial r} = \rho\varepsilon\frac{\partial u}{\partial r}, \tag{16}$$

where, ν is the laminar kinematic viscosity, ε_τ is the turbulent eddy viscosity coefficient, and ε is the total or effective eddy viscosity that takes into account both the laminar and turbulent contributions to the shear stress. While the eddy viscosity hypothesis assumes that momentum transfer in a turbulent flow is dominated by large scale eddies, it also characterizes the mixing due to turbulent fluctuations, which in turn determine the rate of spreading of a free jet.

The eddy viscosity may be derived from the experimental data as follows: Assuming that the evolution of the jet is dependent only on local length and velocity scales and lacks memory of the orifice dimensions itself, the streamwise mean velocity profiles may be considered self-similar. From the conservation of streamwise momentum it may be shown that the characteristic length (b) and velocity (u) of the jet scale as x and x^{-1} respectively. The self-similar assumption then leads to a streamwise velocity profile of the form $u = x^{-1} f\left(\frac{r}{x}\right)$. The similarity variable written as, $\eta = \sigma\frac{r}{x}$, is related to the effective viscosity coefficient through a free constant σ. Since the mixing length hypothesis assumes that the effective viscosity is constant over the entire jet, the boundary layer equations may then be reduced to an ordinary differential equation of the form $ff' = f' - \eta f''$. From the conservation of momentum and the assumed form of the velocity distribution the streamwise velocity is solved to be

$$u = \frac{3K}{8\pi\varepsilon x}\frac{1}{\left(1 + \frac{1}{4}\eta^2\right)^2}, \tag{17}$$

with the self similarity variable given as

$$\eta = \frac{1}{4}\sqrt{\frac{3}{\pi}}\frac{\sqrt{K}}{\varepsilon}\frac{r}{x}, \tag{18}$$

K, the kinematic momentum of the jet, is a measure of the strength of the jet and is obtained as $K = 2\pi\int_0^\infty u^2 r dr$. It is important to note here that the above analysis assumes a constant momentum flux in the streamwise direction. While this is applicable to continuous jets, in synthetic jets it has been reported that the momentum flux at the orifice is higher than that in the far field [1, 31]. The momentum flux was shown to decrease in the near field of the jet due to an adverse pressure gradient, and then asymptote in the far field to some fraction of the exit momentum flux. It is this reduced asymptotic value of the momentum flux that should serve as the magnitude of the driving momentum flux in the above similarity analysis for the synthetic jet, and not the exit momentum flux at the orifice of the actuator.

The eddy viscosity, ε is now obtained from the spreading and decay rates of the jet. At the centerline the streamwise velocity may be expressed as

$$u_c = \frac{3K}{8\pi\varepsilon x} = \frac{1}{S_u x}, \tag{19}$$

where S_u is a measure of the jet decay rate. The radial extent of the jet at a particular axial station may be characterized by a half width ($b_{1/2}$), defined as the radial distance from the centerline at which the streamwise velocity drops to half the centerline velocity. The linear streamwise variation of the half width may be written as

$$b_{1/2} = S_b x, \tag{20}$$

where S_b is the spreading rate of the jet. From Eq. 17 through 20 the free constant σ in the similarity variable is related to the spreading rate as

$$\sigma = \frac{2\sqrt{\sqrt{2}-1}}{S_b}, \tag{21}$$

from which the eddy viscosity is related to the spreading rate and decay rate as

$$\varepsilon = \frac{1}{8\left(\sqrt{2}-1\right)}\frac{S_b^2}{S_u}. \tag{22}$$

In summary, Equation 17 and 22 give the self-similar solution that could be applied to the far field of a turbulent jet: either continuous jet or synthetic jet. Thus, in this study, we are trying employ the same technique as above to extend continuous jet coflow model to synthetic jet.

1.3. Synthetic Jets in a Coflow Wake

As mentioned earlier, similarities between synthetic and continuous turbulent jets motivate extending the model developed in the previous section to synthetic jets. However, three particular differences need to be taken into account before that theory could be applied to synthetic jets in coflow wakes. The first is the increased spreading rate of a synthetic jet in comparison with a counterpart continuous turbulent jet. While a nominal spreading rate for a continuous turbulent jet is about 0.11 [30, 32], the value for a synthetic jet may vary greatly depending on the forcing conditions and upon a non-dimensional operational parameter called the stroke ratio (*L/d*) [1, 13, 33, 34]. The stroke ratio is the ratio of the length of the slug of fluid ejected from the orifice during the expulsion stroke to the diameter of the orifice. It may be obtained through the criteria that the volume displaced by the membrane inside the actuator cavity is equal to the volume ejected from the orifice.

The pulsatile nature of synthetic jets allows for the definition of the characteristic velocity scale to be defined based on either ejected volume or momentum flux of the jet [33, 13]. It is more appropriate

to use the velocity scale based on momentum flux in this study, as the self-similar jet solutions define equivalent jets based on momentum flux rather than mass flux. Thus the velocity scale is given as $U_j = \sqrt{2}\frac{L}{T} = \sqrt{2}fL$, where the associated Reynolds number is defined by

$$Re_{U_j} = \frac{U_j d}{\nu} = \frac{\sqrt{2}fLd}{\nu}. \tag{23}$$

The enhanced spreading rate of a synthetic free jet may be attributed to the enhanced mixing and entrainment of the ambient flow brought about by the periodic introduction, advection, and subsequent interaction of vortical structures [13, 14]. Krishnan and Mohseni [13, 14] showed that the enhanced spreading rate of a synthetic jet could be accounted for by an enhanced eddy viscosity coefficient. They were able to use the jet self-similarity to measure the eddy viscosity coefficient for synthetic jets. To extend the coflow model of section 1.1 to synthetic jets, the spreading rate of a continuous jet (β) must be replaced by that of a synthetic jet in a quiescent environment so that this enhanced spreading rate may be taken into account in the coflow configuration. Systematic measurement of the spreading rate of synthetic free jets are conducted in [13, 14].

The second difference between synthetic and continuous jets which needs to be accounted for lies in the conserved momentum flux assumption in the self-similarity analysis of a jet in a quiescent environment. This translates into the conservation of excess momentum flux in a coflow configuration. This conservation assumption is derived by assuming that there is no pressure gradient in the streamwise direction. While this is more readily applicable to continuous jets, it is not always accurate for synthetic jets. It has been observed that as a result of a pressure gradient near the orifice of the synthetic jet, the momentum flux could decrease in the streamwise direction, reducing to some asymptotic value in the far field [1, 31]. Thus, the above self-similar analysis is applicable after the excess momentum flux reaches a constant value. In this study, the excess momentum flux in equation 3 is obtained from the measured velocity profile downstream of the orifice.

Finally, the theory developed in the previous section assumes that the footprint of the continuous jet actuator is rather small and of the same order of magnitude as the diameter of the pipe issuing the jet. In this case, the wake of the actuator is quite negligible, with minimal effect on the background uniform coflow velocity. This assumption is not really accurate for synthetic jets in a coflow where the entire actuator is required to be placed in the coflow. As a result, the size of the wake behind the synthetic jet actuator scales with the size of the actuator itself instead of the size of the originating jet, i.e., that is the orifice diameter. As a result, the coflow velocity for a synthetic jet can not be treated as a uniform background flow and the effect of the actuator wake needs to be properly accounted for in order to derive a more accurate model.

In this study, the coflow velocities vary in both spanwise and streamwise directions inside the wake region. As discussed in the previous section, the coflow velocity U_a is an important parameter affecting the characteristic length and velocity scales. Therefore, it is natural to define the characteristic coflow velocities for the wake with respect to the wake velocity at different streamwise locations from the actuator. To simplify the characterization of the wake velocity field, the top-hat profile is adopted here and the wake velocity profiles are then averaged while maintaining momentum balance, as shown in Figure 4. The local equivalent coflow velocities for the wake region can then be represented by

$$U_a = \frac{2\pi\int_0^B u_\omega^2 r dr}{2\pi\int_0^B u_\omega r dr}. \tag{24}$$

where u_w is the actuator wake velocity profile measured without the synthetic jet actuator being actuated. It should be noticed that the choice of the integration region for the wake is the same as the jet top-hat width because this region is where the synthetic jet is mostly affected by the coflow wake. After the above modifications are made, the streamwise variation of the non-dimensionalized jet width B^* and centerline velocity U^* of a synthetic jet in a coflow are obtained by solving Equations 13 and 14 numerically. These coupled algebraic equations are discretized first to obtain

$$\frac{B_{i+1}^* - B_i^*}{\Delta x^*} = \sqrt{2}\beta_g \frac{U_i^*}{1+U_i^*}, \tag{25}$$

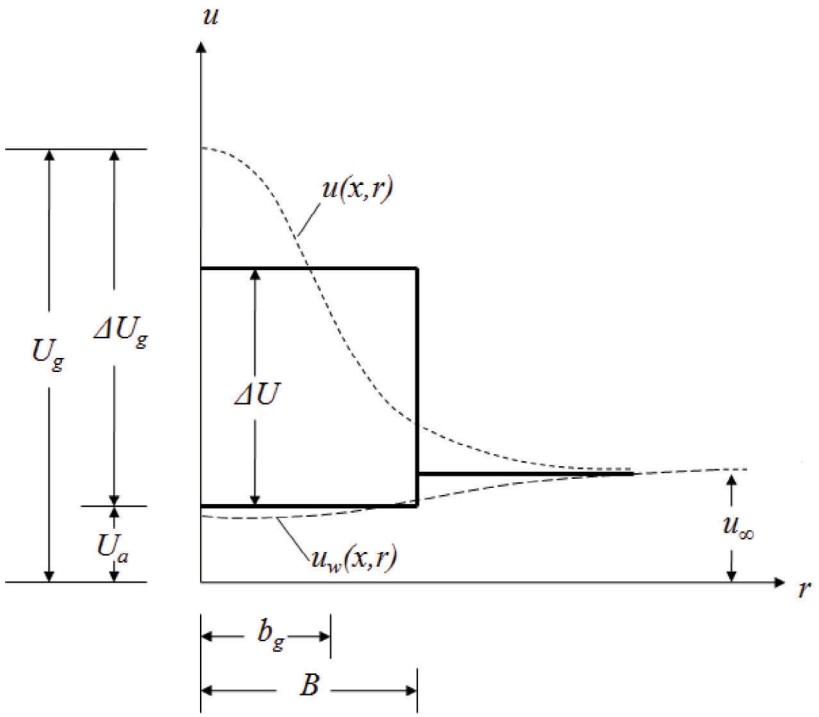

Figure 4: Schematics of the wake velocity profile and the equivalent top-hat jet velocity profile. Note that u_∞ is different from U_a in this case. The coflow wake is also simplified to a top hat profile, $U_a(x)$ with the same width, B, as the velocity profile.

and

$$U_i^* = \frac{-1+\sqrt{1+\frac{4}{\pi B_i^{*2}}}}{2}. \tag{26}$$

here, the negative solution for the velocity is rejected because it is not physically relevant. Then at each position x^*_{i+1}, B^*_{i+1} is computed from Equation 25, in which U^*_i is expressed in terms of B^*_i from Equation 26. Therefore, B^* is actually solved from a single-variable differential equation. In order to solve the above equations, one also needs the initial conditions $U^*(0)$ and $B^*(0)$ at $x^* = 0$, which are obtained experimentally at some designated starting point in the far field. It should be noted that, although this starting point is not rigorously defined, the error of different results computed from different choices of the initial point in the far field is not significant. Considering that there is no external force in the far field of a synthetic jet, the excess momentum flux K_e should be constant. Therefore, the value of K_e is calculated by averaging the local value of K_e over the entire far field data. Moreover, the coflow velocity U_a for a synthetic jet is determined from Equation 24, and then the excess momentum length scale l^* is computed from Equation 4. The spreading rate β_g is determined experimentally in a manner similar to that used for a continuous jet as discussed earlier in this section.

In the following sections, the applicability and validity of these corrections to the model of a continuous jet in a coflow is verified experimentally for a synthetic jet in a coflow wake.

Table 1: Test matrix displaying the driving frequency, f, voltage, V_d, corresponding non-dimensional actuator parameters (L/d, Re_{U_j}), and wind tunnel velocity, U_t.

Case#	*f(Hz)*	*V_d(V)*	*L/d*	*Re_{U_j}*	*U_t(m/s)*
1	2100	30	10.4	4650	1.5
2	2100	30	10.4	4650	2.0
3	2100	30	10.4	4650	2.5
4	2100	25	9.0	4000	1.5
5	2100	20	7.3	3200	1.5

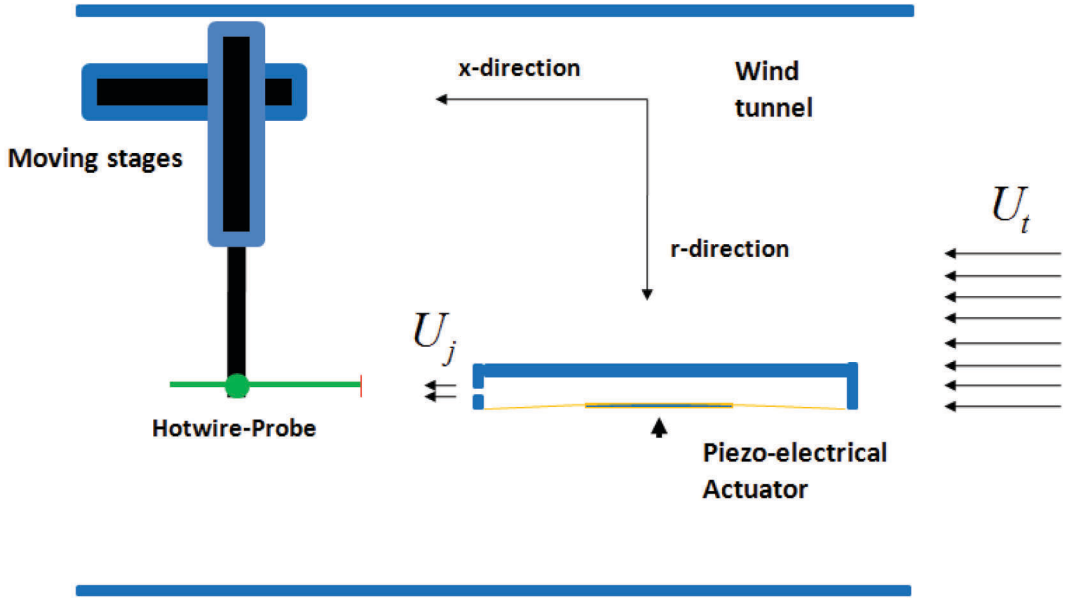

Figure 5: Schematics of the experimental setup displaying a synthetic jet actuator and hot wire probe operating in a wind tunnel. U_t is the wind tunnel velocity and U_j is the jet exit velocity.

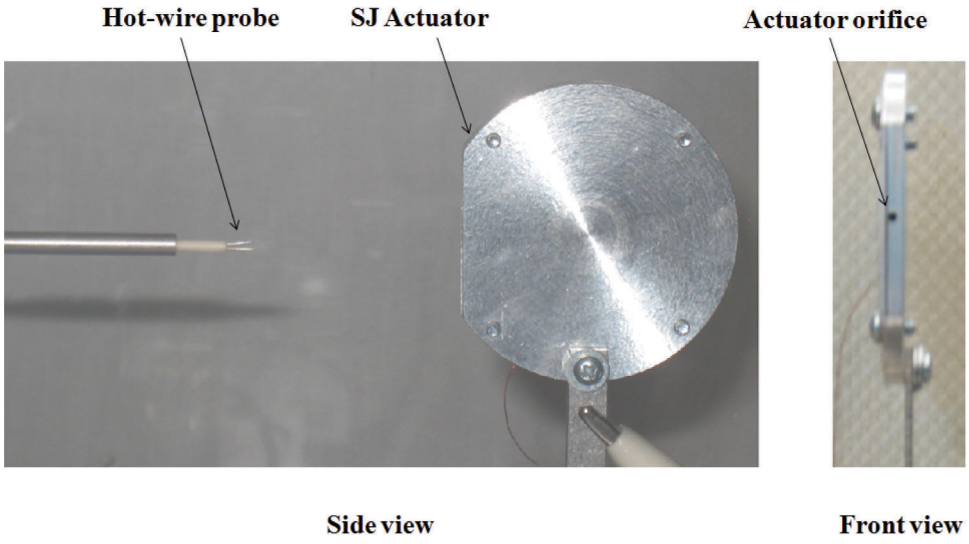

Figure 6: The synthetic jet actuator and hot-wire probe located in the wind tunnel section.

2. EXPERIMENTAL METHOD

The experimental setup to characterize the flow field is comprised of a synthetic jet actuator, automated stages, and a hot-wire anemometry system. Figure 5 shows a schematic of the setup. The experiments are performed in an open circuit wind tunnel with a cross section of 0.34×0.34 *m* and a length of $0.9m$. The wind tunnel speed is varied from 1.5 *m/s* to 2.5 *m/s* for cases 1, 2 and 3 (specified in Table 1) to study the effect of different coflow wakes.

The synthetic jet actuators (see Fig. 6) are designed to have a minimal profile in the direction of the coflow to minimize their wake. The actuator is comprised of a circular piezoelectric disk bounded on a brass shim membrane sandwiched between two circular aluminum elements which form a cavity with an orifice on the side. A flexible membrane is used to seal the cavity. The actuator is 45 *mm* in diameter and 5 *mm* in thickness. The dimensions of the orifice diameter, *d*, and depth are 1.5 *mm* and 0.5 *mm* respectively while the cavity diameter and depth are 35 *mm* and 2 *mm*, respectively. A sinusoidal input voltage drove the piezoelectric membrane, the frequency and amplitude of which are controllable. In this paper, the

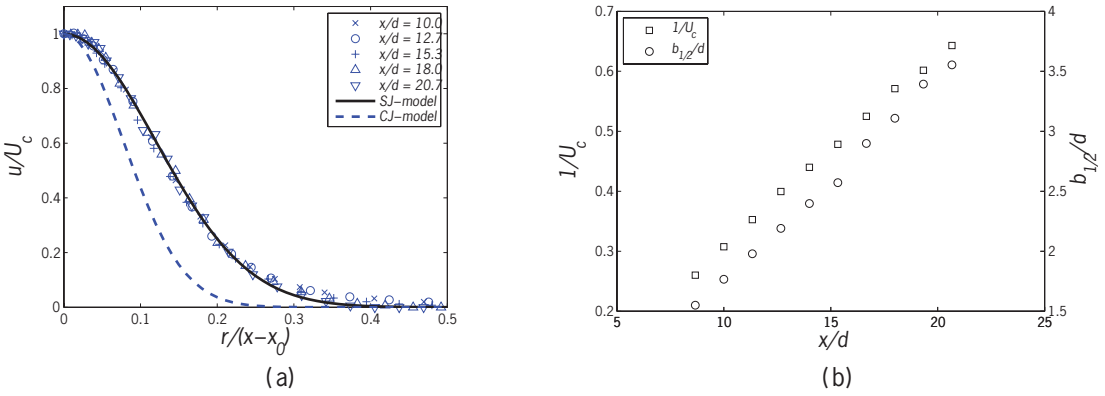

Figure 7: (a) Normalized mean velocity profiles of a synthetic jet actuator associated with the cases 1, 2, and 3 operating in a quiescent environment. $L/d = 10.4$. Our theoretical model for the profile of a synthetic jet (SJ) in a quiescent environment and the velocity profile of a continuous jet (CJ) with similar momentum flux are also shown. (b) The variation of jet half width and centerline velocity for a synthetic jet in quiescent environment, corresponding to the spreading and decay behaviors.

driving frequency, f, is fixed at 2100 *Hz,* which is close to the resonant frequency of the piezo membrane. This causes the membrane to vibrate significantly, thus forming jet flow. The driving amplitude, V_d, is varied from 20 V to 30 V for cases 1, 4 and 5 to study the influence of the jet strength on the overall flow. The test matrix along with the relevant non-dimensional parameters are summarized in Table 1.

The velocity measurements are made using a single normal hot-wire probe operating in constant temperature anemometry (CTA) mode. The measuring element of the hot wire is 1.25 *mm* long and 5 μm in diameter and is aligned such that the prongs are parallel to the axis of the jet. The voltage signal obtained is fed through a low pass filter with a cutoff frequency of 10 kHz. The hot-wire is calibrated in an iterative procedure [35] with a fourth order polynomial curve used to convert voltage to velocity. The hot-wire probe is fixed to a mount positioned on stages capable of being programmed and positioned in the horizontal plane. While traversing the flow field, the stages are moved in discrete intervals, in the streamwise and radial directions, where at each location the flow is sampled for 10 *s*. Based on the accuracy in the calibration and scatter in experimental data, the uncertainty in the mean velocity measurements is estimated to be $\pm 2\%$ for velocities greater than 1.75 m/s, and $\pm 10\%$ for velocities less than 0.75 m/s.

Due to the flow configuration, the presence of the actuator resulted in a wake behind the actuator itself. In order to alleviate this discrepancy most effectively, the actuator is placed in the wind tunnel as shown in Fig. 6. The spanwise direction for the measurement is chosen to be along the thickness of the actuator so that the wake region is minimized.

3. RESULTS & DISCUSSION

3.1. Free Synthetic Jet and Actuator Wake

To serve as a reference, the self-similar nature of synthetic jets corresponding to cases 1, 2, and 3 (i.e., in a quiescent environment with no coflow) is shown in Fig. 7(a). The mean velocity is scaled by the centerline velocity U_c, while the radial coordinate is scaled by the axial distance from the *virtual* origin of the jet ($x - x_0$). The *virtual* origin of a synthetic jet, as defined in [13, 14], is a virtual axial position, where the jet width is zero. This zero-width position is computed from the jet width variation trend in the far field and it is therefore considered as the jet virtual origin in the sense of jet spreading. Much like continuous turbulent free jets, the half width of the synthetic jet increases linearly with x while the centerline velocity decays as x^{-1}, as shown in Fig. 7(b). Additionally, the analytical velocity profiles of the synthetic jet and a high Reynolds number continuous jet are also shown in Fig. 7(a) for comparative purposes. The radial coordinate scaling used allows one to clearly see that the spreading rate of the synthetic jet (0.167 ± 0.003) far exceeds that of a turbulent continuous jet with the same momentum flux (0.109 [21]). This increased spreading is attributed to the enhanced mixing and momentum transfer in a synthetic jet brought about by the periodic pulsation and the enhanced interaction of vortical structures [13, 14]. See Krishnan and Mohseni [13] for the details of synthetic jet modeling in quiescent environment.

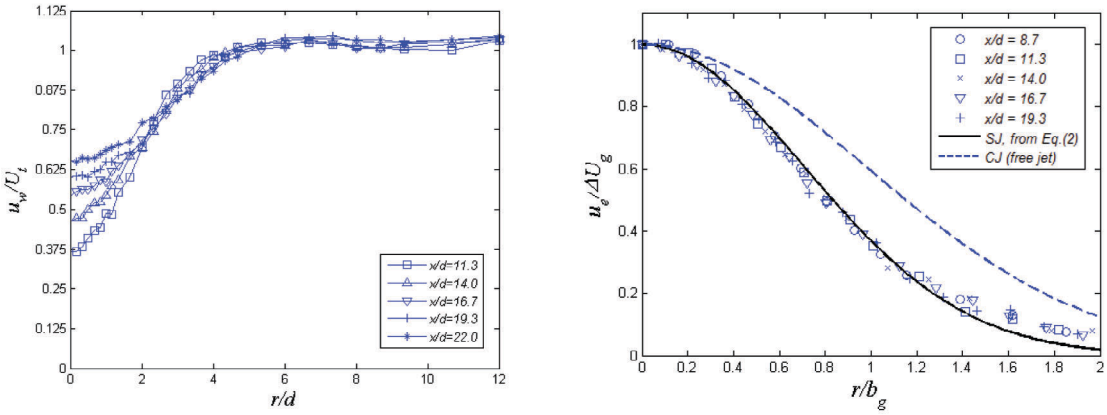

(a) (b)

Figure 8: (a) Normalized wake velocity profiles behind a synthetic jet actuator used in case 1 while the jet is off. $U_t = 1.5m/s$. Note that the actuator is off and this represents the wake velocity profile with no jet. (b) Normalized excess mean velocity profiles of a synthetic jet operating in a coflow wake ($U_t = 1.5m/s$, $L/d = 10.4$). Note that for comparison, the velocity profile for a continuous jet in quiescent environment is also plotted. (b_g in Eq. 2 is computed from the Gaussian profile that fitting the experimental data).

The introduction of a coflow wake changes the mean properties of the synthetic jet as the coflow serves to both contain and advect the jet. To account for the wake after the jet actuator, the velocity field of the coflow wake is tested and the wake profiles corresponding to case 1 are shown in Fig. 8(a) as an example. The scaled collapse of the excess velocity profiles is shown in Fig. 8(b) after subtracting the wake velocities from the coflow jet velocities. As in Eq. 2, the excess velocity is scaled by the centerline excess velocity while the radial distance is scaled by the jet half width. Once again, much like a jet in a quiescent environment, a Gaussian profile approximates the data well except the tail of the profile.

3.2. Coflow Effect

Close to the orifice, the jet velocity will be the dominant velocity scale and the effect of the coflow and wake could be neglected. However, further downstream, where the jet decays and the coflow wake velocity is more pronounced, the excess jet velocity would be comparable to the coflow wake velocity. In this region, the jet exhibits some deviation from the behavior of a jet in a quiescent environment. After experimentally identifying the starting point (x_0^*) of the far field region (see Krishnan and Mohseni for calculating the virtual origin of the jet [13, 14]), $U^*(x^*)$ could be obtained in this region by solving Eq. 13 and Eq. 14 numerically. The result is compared with the experimental data in Fig 9. As seen in Fig. 9, the centerline excess velocity, scaled by the coflow characteristic velocity, is plotted against the axial distance from the jet scaled by the characteristic momentum length scale. It can be observed that the experimentally scaled velocity decay shows good agreement with the theoretical model in all cases. This indicates that our jet spreading hypothesis provides an accurate model of a synthetic jet in a coflow environment. Furthermore, the wake compensation strategy, described in section 1, appears to be an effective technique for defining the relevant coflow velocity and length scales. Moreover, the velocity decay results indicate that the non-dimensional velocity decay of the jet is determined only by the spreading rate of the same jet in a quiescent environment. The different initial points of these curves shows that different coflows affect the initial momentum ratios between the jet and the ambient flow, which is the result of the interaction between the synthetic jet and the coflow in the near field. A weaker coflow velocity could result in a higher initial jet to coflow momentum ratio. However, further downstream, the collapse of the three curves of Figure (9) show that the properly scaled velocities decay similarly albeit the changes in the coflow velocity.

Figure 10(a) shows the variation of the half width of the synthetic jet with the streamwise distance. As seen, all cases of the synthetic jet in a coflow wake studied here show a linear trend in the jet width variation, just as was found for a free synthetic jet in our previous work [13]. However, it is noted that whereas our previous study of the continuous jet in uniform coflow [21] found that the spreading of the jet shows a nonlinear trend over the region $x/l^* < 18$ that the slope of the jet width significantly

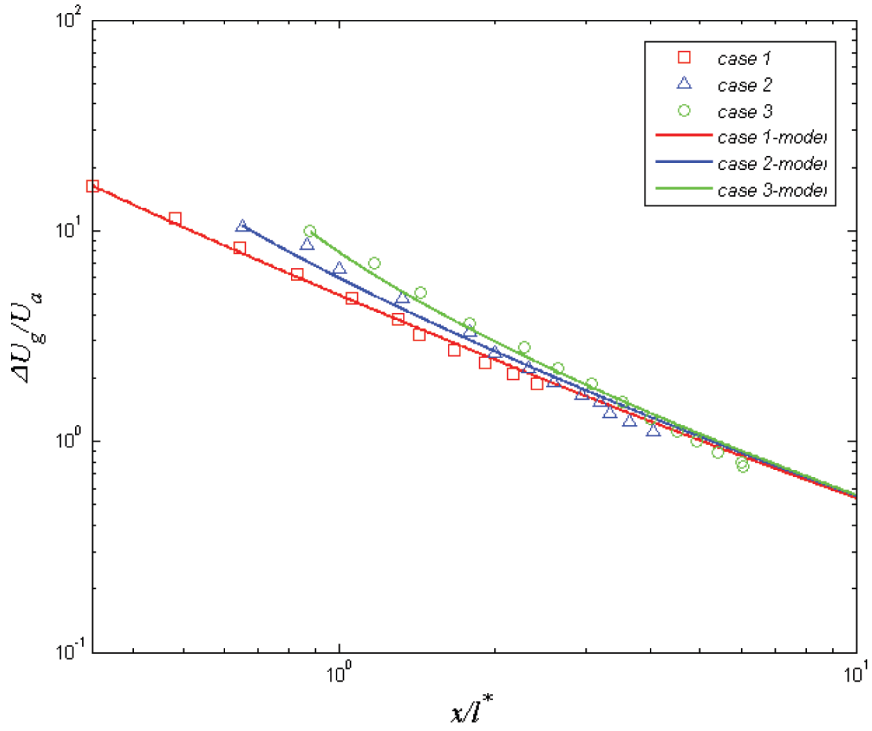

Figure 9: Normalized centerline velocity decay ($\Delta U_g/U_a$) as a function of the scaled streamwise distance (x/l^*) for cases 1, 2 and 3. Analytical solution for synthetic jets (SJ) solved from our model in equations 13 and 14 is also plotted for comparison.

deflected at the region $x/l^* > 10$; in this investigation, the flow field is measured over a region corresponding to $x/l^* < 8$, and so the spreading of the synthetic jet may still be treated as linear. This indicates that the spreading of a synthetic jet in a coflow wake may be characterized by a single constant coefficient, namely the spreading rate (β_g). Figure 10(b) shows the corresponding spreading rates for the three cases considered. Here, the coflow variation is accounted for by a momentum flux ratio (U_j^2/U_t^2), which is the ratio of the synthetic jet exit average momentum flux to the average coflow momentum flux. In these three cases, U_t is varied while U_j remains constant. From observation, it is clear that the spreading rates of synthetic in coflow are smaller than that of a same synthetic in

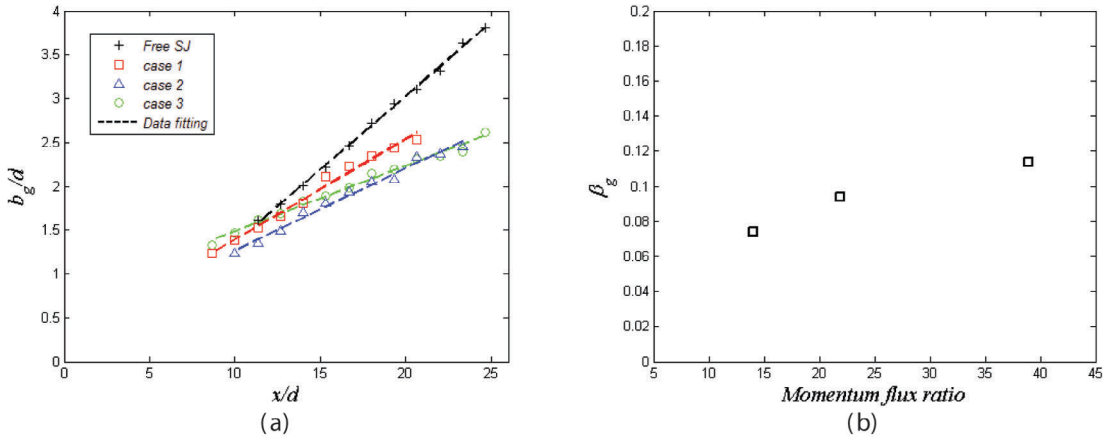

Figure 10: (a) Jet half width, b_g, as a function of the non-dimensional streamwise distance x for cases 1, 2, 3 and free synthetic jet; (b) Spreading rate change with coflow wake. The coflow velocity is converted to momentum flux ratio and expressed as (U_j/U_t) . Note that β_g for synthetic jets with $U_t = 0$ (quiescent environment, corresponding to infinity in this diagram), is 0.167.

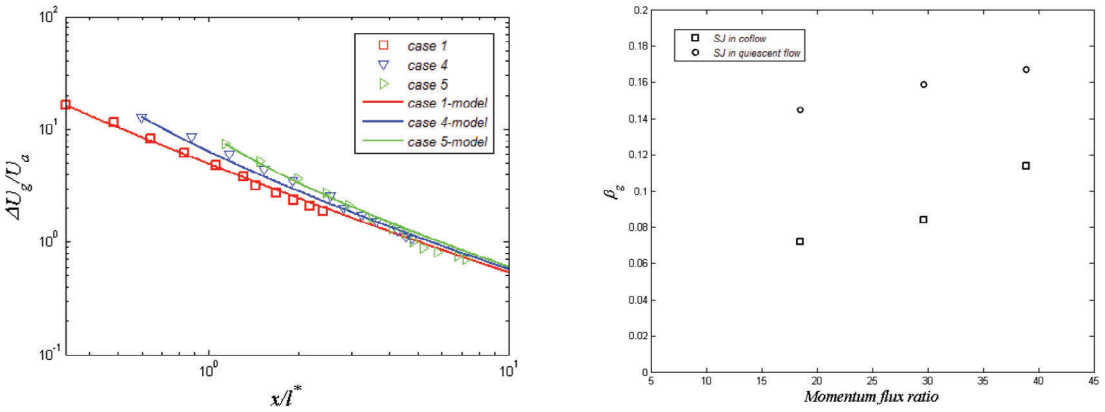

(a) (b)

Figure 11: (a) Normalized centerline velocity decay as a function of the scaled streamwise distance for cases 1, 4 and 5; (b) Spreading rate change with the jet strength for synthetic jet in coflow wake. The spreading rates of the synthetic jets with the same jet strengths with no coflow are also shown for comparison. The jet strength is converted to momentum flux ratio, which is expressed as $(U_j/U_t)^2$.

quiescent flow. Further observation indicates that the presence of the coflow decreases the spreading of the synthetic jet to values that are even smaller than that of the spreading rate for a free continuous jet. Another point to note is that the spreading rate decreases as the coflow velocity increases. A possible explanation for this is that the existence of the coflow reduces the relative velocity jump across the shear layer of the jet and results in less shear layer energetics and less entrainment of the ambient flow by the jet; therefore, causing a weaker spreading of the jet.

3.3. Effect of Jet Strength

Besides the magnitude of the coflow wake velocity, the strength of the synthetic jet itself also plays a role in characterizing the flow. Here, the synthetic jet strength is changed by adjusting the input voltage, and the resultant strength may be characterized either using the value of L/d or the momentum flux ratio (U_j^2/U_t^2). The larger the momentum flux ratio the higher the jet strength. Figure 11(a) shows the centerline excess velocity decay with streamwise distance for different strengths of the synthetic jet in the same coflow wake. Again, the experimental data shows good agreement with the theoretical model. This verifies the validity of our previous hypothesis and assumptions made to extend the continuous jet model to synthetic jets in coflow wake. A comparison of the velocity decay plots for several cases shows that a stronger jet decays faster than a weaker one in the same coflow. Furthermore, stronger jets have larger initial momentum ratios with respect to the coflow. This faster decay rate of stronger synthetic jets can be attributed to a larger velocity difference between the jet and the ambient coflow, which causes the jet to entrain more fluid. The spreading rates for synthetic jets with and without a coflow are shown in Figure 11(b). These results confirms our previous observation that the coflow would decrease the spreading rate of a synthetic jet. Like the trend of synthetic jets in quiescent flow, a stronger jet increases the spreading rate of the synthetic jet. As stated previously, this is caused by the enhanced mass entrainment from the ambient. It should be noted that, although adjusting the jet strength or the coflow velocity would both change the initial momentum ratio and affect the jet spreading and decay, it is actually the jet strength that determines the spreading and decay rate while the coflow affects only the initial condition and the velocity and length scales.

4. CONCLUSIONS

The flow field of a synthetic jet in a background flow is investigated using hot wire anemometry. An integral model similar to that employed in modeling continuous jets in a coflow is shown to be applicable to synthetic jets with some adjustments for the enhanced spreading rate of a synthetic jet and a wake compensation for the flow actuator. The excess velocity profile of a synthetic jet in a coflow demonstrates self-similar behavior when scaled with the characteristic velocity and length scales obtained from a calculated top hat velocity profile. The model for the streamwise velocity decay shows good agreement with experimental data for different coflow velocities and jet strengths. This model indicates that, in the

far field, the non-dimensional velocity decay of a synthetic jet in a coflow is mostly determined by the spreading rate of that synthetic jet in quiescent environment. The effect of different coflow velocities on this model is reflected by the different initial values of the non-dimensional velocities at the beginning of the far field. The observed decrease in the spreading rate of the jet indicates that the existence of the coflow decreases the spreading of the synthetic jet. Furthermore, increasing the jet strength, parametrized by increasing L/d in this study, causes an enhancement in jet spreading. The model presented here can be used to model the mean characteristics of a synthetic jet issues into a coflow wake.

ACKNOWLEDGEMENTS

The authors would like to thank Gopi Krishnan for his contribution of establishing the previous theory. The authors would like to thank Matthew Shields and Jill Cooper for their help in post-editing. The authors would like to acknowledge partial support from the Air Force Office of Scientific Research.

REFERENCES

[1] Smith, B. and Glezer, A., 1998, "The formation and evolution of synthetic jets," Phys. Fluids, **10**(9), pp. 2281–2297.

[2] Glezer, A. and Amitay, M., 2002, "Synthetic jets," Ann. Rev. Fluid Mech., **34**, pp. 503–529.

[3] Seifert, A., Eliahu, S., Greenblatt, D., and Wygnanski, I., 1998, "Use of piezoelectric actuators for airfoil separation control," AIAA Journal, **36**(8), pp. 1535–1537.

[4] Amitay, M., Smith, D. R., Kibens, V., Parekh, D., and Glezer, A., 2001, "Aerodynamic flow control over an unconventional airfoil using synthetic jet actuators," AIAA Journal, **39**(3), pp. 361–370.

[5] Mohseni, K., 2006, "Pulsatile vortex generators for low-speed maneuvering of small underwater vehicles," Ocean Engineerings, **33**(16), pp. 2209–2223.

[6] Krieg, M. and Mohseni, K., 2008, "Thrust characterization of pulsatile vortex ring generators for locomotion of underwater robots," IEEE J. Oceanic Engineering, **33**(2), pp. 123–132.

[7] Mohseni, K., 2001, "Guided capsule for wireless endoscopy, biopsy, and drug delivery," Patent.

[8] Mohseni, K., 2007, "An steerable mechanism for wireless capsule endoscopy," *Proceedings of the 2nd Frontiers in Biomedical Devices Conference*, ASME, Irvine, CA, pp. BioMed 2007–38048.

[9] Honohan, A. M., Amitay, M., and Glezer, A., 2000, "Aerodynamic control using synthetic jets," AIAA paper 2000–2401, Fluids 2000 Conference and Exhibit, Denver, CO.

[10] Mittal, R. and Rampunggoon, P., 2002, "On the virtual aeroshaping effect of synthetic jets," Phys. Fluids, **14**(4), pp. 1533–1536.

[11] Whitehead, J. and Gursul, I., 2006, "Interaction of synthetic jet propulsion with airfoil aerodynamics at low reynolds numbers," AIAA J., **44**(8), pp. 1753–1766.

[12] Rizetta, D. P., Visbal, M. R., and Stanek, M. J., 1998, "Numerical investigation of synthetic jet flow-fields," AIAA Paper 98–2910.

[13] Krishnan, G. and Mohseni, K., 2009, "Axisymmetric synthetic jets: An experimental and theoretical examination," AIAA J., **47**(10), pp. 2273–2283.

[14] Krishnan, G. and Mohseni, K., 2009, "An experimental and analytical investigation of rectangular synthetic jets," ASME J. Fluid Eng., **131**(12).

[15] Ugrina, S., 2007, *Experimental analysis and analytical modeling of synthetic jet cross flow interaction*, Ph.D. thesis, University of Maryland.

[16] Xia, X. and Mohseni, K., 2010, "Modeling and experimental investigation of synthetic jets in cross-flow," AIAA paper 2010-0106, 48th AIAA Aerospace Sciences Meeting Including the New Horizons Forum and Aerospace Exposition, Orlando, FL.

[17] Krueger, P., Dabiri, J., and Gharib, M., 2006, "The formation number of vortex rings formed in a uniform background co-flow," Journal of Fluid Mechanics, **556**(1), pp. 147–166.

[18] Mallinson, S., Hong, G., and Reizes, J., 1999, "Some characteristics of synthetic jets," AIAA paper 1999–3651, Norfolk, VA, proceedings of the 30th AIAA Fluid Dynamics Conference.

[19] Antonia, R. and Bilger, R., 1973, "Experimental investigation of an axisymmetric jet in a co-flowing air stream," J. Fluid Mech, **61**, pp. 805–822.

[20] Nickels, T. and Perry, A., 1996, "An experimental and theoretical study of the turbulent coflowing jet," J. Fluid Mech, **309**, pp. 157–182.

[21] Chu, P., Lee, J., and Chu, V., 1999, "Spreading of turbulent round jet in coflow," Journal of Hydraulic Engineerings, **125**, pp. 193–204.

[22] Squire, H. and Trouncer, J., 1944, "Round jets in a general stream," Tech. rep., Aero Research Council, London, UK.

[23] Hill, P., 1965, "Turbulent jets in ducted streams," J. Fluid Mech, **22**, pp. 161–186.

[24] Patel, R., 1971, "Turbulent jets and wall jets in uniform streaming flow," Aeronautical Quarterly, **22**, pp. 311–326.

[25] Morton, B., 1962, "Coaxial turbulent jets," Int. J. Heat Mass Transfer, **5**, pp. 955–965.

[26] Maczynski, J., 1962, "A round jet in an ambient co-axial stream," J. Fluid Mech, **13**, pp. 597–608.

[27] Krishnan, G. and Mohseni, K., 2010, "An experimental study of a radial wall jet formed by the normal impingement of a round synthetic jet," European Journal of Mechanics B/Fluids, **29**, pp. 269–277.

[28] Kotsovinos, N. and Angelidis, P., 1991, "The momentum flux in turbulent submerged jets," J. Fluid Mech, **229**, pp. 453–470.

[29] Schlichting, H., 1933, "Laminare strahlausbreitung," J. Appl. Math. Mech. (ZAMM), **13**, pp. 260–263.

[30] Schlichting, H., 1979, *Boundary-Layer Theory*, McGraw-Hill Book Company, New York.

[31] Fugal, S. R., Smith, B. L., and Spall, R. E., 2005, "Displacement amplitude scaling of a two-dimensional synthetic jet," Physics of Fluids, **17**(4), pp. 045103–1–10.

[32] Pope, S., 2000, *Turbulent Flows*, Cambridge University Press, New York.

[33] Smith, B. and Swift, G., 2001, "Synthetic jets at larger reynolds number and comparison to continuous jets," AIAA paper AIAA 2001-3030, Anaheim, CA, 31st AIAA Fluid Dynamics Conference and Exhibit.

[34] Shuster, J. and Smith, D., 2007, "Experimental study of the formation and scaling of a round synthetic jet," Physics of Fluids, **19**(4), pp. 45109–1–21.

[35] Johnstone, A., Uddin, M., and Pollard, A., 2005, "Calibration of hot-wire probes using non-uniform mean velocity profiles," Experiments in Fluids, **39**(3), pp. 525–532.